Study of the benzene·N_2 intermolecular potential-energy surface

Soohyun Lee, Joann Romascan, and Peter M. Felker
Department of Chemistry and Biochemistry, University of California, Los Angeles, California 90095-1569

Thomas Bondo Pedersen,[a] Berta Fernández, and Henrik Koch[a]
Department of Physical Chemistry, University of Santiago de Compostela, E-15706 Santiago de Compostela, Spain

(Received 23 September 2002; accepted 17 October 2002)

The intermolecular potential-energy surface pertaining to the interaction between benzene and N_2 is investigated theoretically and experimentally. Accurate intermolecular interaction energies are evaluated for the benzene–N_2 van der Waals complex using the coupled cluster singles and doubles including connected triples [CCSD(T)] method and the aug-cc-pVDZ basis set extended with a set of $3s3p2d1f1g$ midbond functions. After fitting the energies to an analytic function, the intermolecular Schrödinger equation is solved to yield energies, rotational constants, and Raman-scattering coefficients for the lowest intermolecular levels of several benzene–N_2 isotopomers. Experimentally, intermolecular Raman spectra of jet-cooled h_6- and d_6-benzene–N_2 measured at 0.03 cm^{-1} resolution by mass-selective, ionization-detected stimulated Raman spectroscopies are reported. Seven intermolecular bands are assigned for each isotopomer, including transitions involving intermolecular bending and stretching vibrations and internal rotation about the benzene C_6 axis. These Raman data, together with measured rotational constants and binding energies obtained by other groups on benzene–N_2, agree well with the theoretical results. Such agreement points to the promise of the quantum chemical methodology employed herein in future investigations of larger van der Waals complexes. © *2003 American Institute of Physics.*
[DOI: 10.1063/1.1527925]

I. INTRODUCTION

Characterization of the intermolecular level structures of molecular complexes and clusters can lead to detailed knowledge of intermolecular potential-energy surfaces (IPSs) and of dynamics in multimolecule systems.[1,2] In such an endeavor a comprehensive approach consisting of (a) experimental measurements, (b) calculations of IPSs, and (c) dynamically-exact calculations of intermolecular states can be very valuable: The highly-coupled, large-amplitude motions that are often associated with intermolecular states lead to significant complications in the extraction of useful information from experimental results, complications that require close coupling between experiment and computations in order to be overcome.

In the calculation of IPSs, advances in computational methods and increases in computing power in recent years have made it possible to use *ab initio* electronic structure methods to calculate intermolecular interaction energies over a sufficient number of grid points to permit the generation of fitted IPS functions, accurate on a wave number scale, for molecule–atom and molecule–molecule van der Waals complexes (e.g., Refs. 3–7). At the same time, significant advances have also been made in solving, without dynamical approximations apart from the rigid-monomer approximation, the intermolecular rotation-vibration-tunneling Schrödinger equation, given an assumed IPS (e.g., Refs. 8 and 9). The upshot is that it is now feasible to make direct comparison between experiment and first-principles theory for van der Waals species with as many as six intermolecular degrees of freedom.

The principal purpose of this paper is to make such a comparison for the benzene–N_2 complex. This species is of interest for several reasons. First, it is a convenient model system for investigating the details of physisorption interactions between N_2 and aromatic surfaces. Second, it represents the next step up in complexity relative to atom–polyatomic van der Waals species in the investigation of intermolecular forces and dynamics. Besides the dispersion/exchange-repulsion interactions that dominate in contributing to the intermolecular force-field of the former species, there are significant electrostatic contributions to the benzene–N_2 force field, contributions that often play a central role in the interactions between π-electron systems. Further, the five-dimensional nature of the intermolecular problem in benzene–N_2 leads to qualitatively different intermolecular dynamics (e.g., internal-rotation and torsional motions) than is possible in atom–molecule systems. Third, the complex's high symmetry facilitates calculations of its IPS and of its intermolecular level structure. Finally, the species has been studied spectroscopically by several different groups. Indeed, there are experimental results pertaining to its vibronic spectroscopy,[10,11] rotational level structure,[11,12] binding energy,[13] and intra-,[14] and intermolecular[15] vibrational spectroscopy.

[a]Present address: Institute of Molecular Science, Department of Physical Chemistry, University of Valencia, Dr. Moliner 50, E-46100 Burjassot (Valencia), Spain.

The outline of the paper is as follows: In the next section we present the results of *ab initio* calculations aimed toward elucidating the IPS of the complex. These calculations go beyond prior work on the complex[16–18] in two ways: First, the number of grid points considered (198) is larger. Second, the level of the calculation is higher. Indeed, it is at a level shown to yield wave-number-accurate intermolecular vibrational results for the benzene–Ar complex.[3–5] In Sec. III we describe the fit of the *ab initio* results to an analytic IPS function and present the results of that fit. Section IV pertains to the calculation, by the procedures of Ref. 19, of the intermolecular states of benzene–N_2 for the IPS of Sec. III. Results relating to the $J=0$ level structure, the rotational constants of selected vibrational states, and intermolecular vibrational Raman scattering activities are presented. Section V outlines experimental procedures employed to obtain nonlinear Raman spectroscopy data on the intermolecular transitions of the complex. New, more extensive results from such experiments are then presented in Sec. VI. These results go a long way toward characterizing the low-energy intermolecular level structure of benzene–N_2 and toward confirming the accuracy of the theoretical results. Section VII is a concluding section.

II. *AB INITIO* CALCULATIONS

The *ab initio* calculation of van der Waals IPSs within the Born–Oppenheimer approximation is a formidable task. The number of grid points needed is often prohibitive in itself, as the entire surface must be covered in order to allow for the large-amplitude intermolecular modes typical of weakly bound complexes. Furthermore, highly correlated levels of size-extensive electronic structure theory accompanied by relatively large atomic basis sets are imperative for accurately calculating the interaction energies. Subscribing to the supermolecular approach, interaction energies are computed as the difference between the complex energy and the sum of monomer energies. Accounting for the inherent basis set superposition error via the counterpoise correction[20] implies that three separate *ab initio* calculations are needed for each grid point, thus making the total number of computations thrice the number of grid points. Moreover, the counterpoise correction scheme simultaneously enlarges the size of the basis set and reduces the point group symmetry, thereby increasing the computational effort for the monomer calculations.

In the spirit of the Born–Oppenheimer approximation underlying the concept of an IPS, we choose to fix the nuclear conformations of the benzene and N_2 moieties at values determined from rotational analysis of experimental spectroscopic data. The benzene molecule is kept in the planar D_{6h} geometry with $R_{CC}=1.397$ Å and $R_{CH}=1.080$ Å,[21] and for the nitrogen molecule $R_{NN}=1.0977$ Å.[22] The number of ''active'' internal nuclear coordinates consequently reduces to the five intermolecular ones, thus effectively decoupling the intra- and intermolecular modes of nuclear motion. This approximation is justifiable by the large differences between typical frequencies of intra- and intermolecular vibrations. However, even with this reduction of the IPS dimension, we are faced with a devastating computational effort for a reasonably uniform grid. To further reduce the dimension of the grid we initially focus on points with symmetry, i.e., at least C_S point group symmetry, followed by a limited set of computationally more expensive no-symmetry points chosen from a preliminary fit to an analytical expression. The higher symmetry points initially considered are comprised of those for which the N_2 center-of-mass is located on one of the benzene principal axes of inertia with the vector connecting the nitrogen nuclei parallel to the same or to another of these axes, giving nine series of grid points. The additional points are chosen in the neighborhood of the global minimum of the preliminary fit. See Ref. 23 for the full set of 198 grid points calculated in the present study.

In previous work,[3–7] the coupled cluster singles and doubles including connected triples model [CCSD(T)] (Ref. 24) in conjunction with augmented correlation consistent polarized valence atomic basis sets has been shown to provide sufficient correlation treatment to describe the demanding electronic structure of similar van der Waals complexes. Particularly relevant for our purposes, recent studies of the ground and first singlet excited state IPSs of the benzene–Ar complex[3–5] have demonstrated the adequacy of the CCSD(T) model along with the aug-cc-pVDZ basis set extended with a $3s3p2d1f1g$ (henceforth denoted 33211) set of bond functions for theoretically generating rovibrational spectra in quantitative agreement with available experimental results. Therefore, without further testing, we employ the CCSD(T) model and the aug-cc-pVDZ-33211 basis set (see, e.g., Ref. 3 for the exponents defining the 33211 set) for calculating the ground state interaction energies of the benzene–N_2 complex. For each grid point, the bond functions are placed in the middle of the vector joining the centers-of-mass of the benzene and N_2 molecules. All interaction energies are counterpoise corrected[20] and calculated in the frozen core approximation using the DALTON program.[25–27] Despite the various approximations described above, the total computational cost of generating the grid exceeds 24 months of CPU time using a variety of computer architectures, illustrating both the capabilities and limitations of state-of-the-art quantum chemistry.

As outlined in the following section, only 37 low-energy geometries from the complete set of 198 addressed by the *ab initio* calculations were used in generating a fitted IPS function. The calculated energies for these geometries are presented in Table I. In the table the geometries are specified by coordinates referred to the body-fixed axis system $BF_1 \equiv (\hat{x}_1, \hat{y}_1, \hat{z}_1)$, which is centered at the complex's center-of-mass and has $\hat{z}_1$ parallel to the benzene C_6 axis and pointing away from the benzene moiety, $\hat{x}_1$ parallel to the bisector of the bond between carbon #1 and carbon #2 of benzene, and $\hat{y}_1$ so as to complete a right-handed coordinate system. The specific coordinates are (a) z, ρ, and Φ, the cylindrical coordinates in BF_1 of the vector from the benzene center-of-mass to the nitrogen center of mass and (b) ϕ and θ, the polar angles that specify the orientation of the N_2 internuclear axis relative to BF_1.

TABLE I. Benzene–N_2 grid points and *ab initio*-calculated interaction energies. Interaction energies (V, V_{fit}) are given in cm^{-1}, distances (z, ρ) in Å, and angles (Θ, Φ, θ, and ϕ) in degs.

z	ρ	Φ	θ	ϕ	V^a	$V_{\text{fit}}-V$
4.000 00	0.000 00	0.0	90.0	0.0	−356.285 80	−3.635
3.750 00	0.000 00	0.0	90.0	0.0	−443.593 18	1.886
3.600 00	0.000 00	0.0	90.0	0.0	−487.996 54	2.919
3.500 00	0.000 00	0.0	90.0	0.0	−506.645 01	1.987
3.450 00	0.000 00	0.0	90.0	0.0	−510.431 87	1.041
3.400 00	0.000 00	0.0	90.0	0.0	−509.169 06	−0.120
3.350 00	0.000 00	0.0	90.0	0.0	−501.595 30	−1.311
3.300 00	0.000 00	0.0	90.0	0.0	−486.216 21	−2.224
3.250 00	0.000 00	0.0	90.0	0.0	−461.268 55	−2.367
3.200 00	0.000 00	0.0	90.0	0.0	−424.770 84	−0.908
3.150 00	0.000 00	0.0	90.0	0.0	−374.003 28	2.954
4.000 00	0.000 00	0.0	90.0	90.0	−356.164 37	−3.757
3.850 00	0.000 00	0.0	90.0	90.0	−408.920 38	−0.161
3.700 00	0.000 00	0.0	90.0	90.0	−459.570 05	2.279
3.600 00	0.000 00	0.0	90.0	90.0	−487.732 23	2.637
3.500 00	0.000 00	0.0	90.0	90.0	−506.341 48	1.651
3.400 00	0.000 00	0.0	90.0	90.0	−508.827 16	−0.521
3.300 00	0.000 00	0.0	90.0	90.0	−485.838 77	−2.709
3.200 00	0.000 00	0.0	90.0	90.0	−424.270 85	−1.607
3.150 00	0.000 00	0.0	90.0	90.0	−373.591 29	2.271
3.450 00	0.000 00	0.0	90.0	15.0	−510.265 66	0.852
3.450 00	1.224 74	45.0	90.0	15.0	−351.420 51	3.095
3.450 00	0.000 00	0.0	80.0	15.0	−492.481 15	1.139
3.450 00	0.750 00	0.0	80.0	15.0	−418.530 43	−0.832
3.450 00	0.750 00	90.0	90.0	15.0	−429.143 47	−0.433
3.450 00	0.250 00	0.0	90.0	0.0	−501.117 41	0.232
3.450 00	0.750 00	0.0	90.0	0.0	−437.358 87	−1.165
3.450 00	0.750 00	90.0	80.0	15.0	−409.034 75	0.977
3.450 00	0.750 00	0.0	90.0	15.0	−436.528 99	−1.505
3.450 00	0.250 00	90.0	90.0	90.0	−500.860 36	−0.195
3.450 00	0.750 00	90.0	90.0	90.0	−437.106 41	−3.154
3.450 00	0.250 00	0.0	90.0	15.0	−500.872 81	0.063
3.450 00	0.250 00	90.0	90.0	15.0	−499.663 61	0.376
3.450 00	0.750 00	90.0	90.0	0.0	−428.952 31	−0.018
3.450 00	0.250 00	90.0	90.0	0.0	−499.752 94	0.576
3.450 00	0.750 00	0.0	90.0	90.0	−428.136 37	−1.406
3.450 00	0.250 00	0.0	90.0	90.0	−499.362 10	0.248

[a]We have employed the following conversion factors: 1 bohr = 0.529 177 25 Å, 1 hartree = 219 474.625 cm^{-1}.

III. FITTED INTERMOLECULAR POTENTIAL-ENERGY SURFACE

A. IPS function

Ab initio energies computed as described in the preceding Section were fit to an IPS function consisting of two parts,

$$V \equiv V_1 + V_2 . \tag{3.1}$$

The V_1 part contains atom–atom 6–12 terms between the nonbonded atoms on the benzene and the N_2 moieties, as well as N–C–C three-body terms,

$$V_1 = \sum_i \left[v_C \left(\sum_j u_C^2(r_{ij}) + w \sum_{j>k} u_C(r_{ij}) u_C(r_{ik}) \right) + v_H \sum_l u_H^2(r_{il}) \right] - v_C(12+30w) - 12 v_H , \tag{3.2}$$

where the indices i, j, k, and l run over the N, C, C, and H atoms, respectively, r_{ij} is the distance between atom i and j, $u_C(r) \equiv 1-(r_C/r)^6$, $u_H(r) \equiv 1-(r_H/r)^6$, and v_C, r_C, v_H, r_H, and w are fitting parameters. V_1 is a slight modification of the functional form employed by Brupbacher *et al.*[28] in their representation of the IPS of benzene–Ar. The V_2 part contains coulombic interaction terms between charge centers on the nitrogen and benzene. The charge centers on the benzene were taken to be at the positions of the carbon and hydrogen nuclei. All the carbons were taken to have the same charge, and all the hydrogens were taken to have charges equal and opposite to those of the carbons. On the nitrogen molecule three charge centers were used. One was taken to be at the molecule's center-of-mass. The other two were taken to be at the positions of the nitrogen nuclei. The latter two charges were assumed to be equal, and the third was taken to be opposite to these with twice their magnitude. Hence,

$$V_2 = q_{NC} \left[2 \left(\sum_j \frac{1}{r_j} - \sum_l \frac{1}{r_l} \right) - \sum_i \left(\sum_j \frac{1}{r_{ij}} - \sum_l \frac{1}{r_{il}} \right) \right], \tag{3.3}$$

where i, j, and l have the same meaning as in Eq. (3.2), r_j and r_l are the distances between the center charge on the N_2 and the jth carbon and lth hydrogen, respectively, and q_{NC} is a fitting parameter. Note that because of the symmetry of the assumed charge distributions, only one independent charge parameter, q_{NC}, is required to specify the Coulombic interaction. Note further that $2q_{NC}$ represents the product of the charge on a carbon with that at the center of the nitrogen molecule. Based on a consideration of the quadrupole moments of the dinitrogen[29] and benzene[30] moieties, one would expect this parameter to be negative (the carbon charge should be negative and that at the center of the N_2 should be positive). Finally, note that V is such that the zero of the potential corresponds to infinitely separated benzene and N_2 moieties.

TABLE II. Potential-energy parameters for benzene–N_2 calculations.

$v_C = 68.7152\ \text{cm}^{-1}$	$r_C = 3.7559$ Å	$w = -0.271\ 38$
$v_H = 30.4110\ \text{cm}^{-1}$	$r_H = 3.4235$ Å	$q_{NC} = -0.067\ 356$ a.u.

B. Fitting procedure and results

A nonlinear least-squares method employing Marquardt's algorithm[31] was used to fit V from Eq. (3.1) to the *ab initio*-calculated energies. Only *ab initio* energies less than a predetermined cut-off were included in any given fit. For the final fitted function used herein the energy cut-off was chosen to be $-330\ \text{cm}^{-1}$, giving rise to the 37 point *ab initio* data set of Table I. The best-fit parameters resulting from this fit are given in Table II. The quality of the fit, as measured by the root-mean-square deviation between *ab initio* and fit energies, is $2\ \text{cm}^{-1}$. A direct comparison between *ab initio* energies and those from the fitted function is given in Table I. Significant deterioration in the quality of fits (e.g., greater than twofold increases in root-mean-square deviation) was found to occur for energy cut-off values higher than $-300\ \text{cm}^{-1}$. This was largely due to the inability to fit accurately the energies for those geometries having $0 < \theta$

$<45°$. One suspects that inadequate modeling of electrostatic and/or the exchange-repulsion interactions in V of Eqs. (3.1)–(3.3) is responsible for this, an inadequacy that might be addressed in future studies with a more flexible IPS function. In any case, because of this deterioration in fit quality the -330 cm^{-1} value was employed for the cut-off. Notably, this energy is 180 cm^{-1} above the minimum on the *ab initio* surface and (as detailed below) is about 74 cm^{-1} above the computed intermolecular zero-point energy of the complex. One therefore expects results obtained with the fitted function to be most accurate in the low-energy region of the intermolecular level structure, the region that is relevant to almost all existing experimental results.

While no claim of uniqueness can be made for the best-fit parameter values of Table II, it is pertinent to examine whether they are reasonable. Comparing the values of v_C, r_C, and w with their analogs from the benzene–rare gas studies of Brupbacher *et al.*,[28] one finds that the former are in the same range as the latter. Comparing v_C and v_H, one notes that the factor-of-2 or so difference between them is that which might be expected given literature values of Lennard-Jones parameters for N–C and N–H interactions.[32] Finally, the value of q_{NC} has the expected negative sign (see above) and has a magnitude that suggests partial charges on the order of 0.2 a.u. at the various charge centers, a value that is in rough accord with calculations of charge distributions in the monomers.

C. Characteristics of the fitted IPS

The fitted IPS obtained by using Eqs. (3.1)–(3.3) and the parameters of Table II has six equivalent global minima at -510.036 cm^{-1} corresponding to geometries in which (a) the N_2 moiety's center-of-mass is on the C_6 axis of benzene at a distance of $R=3.425$ Å from the plane of the latter moiety, (b) the N_2 is oriented with its internuclear axis parallel to the benzene plane, and (c) the projection of the N_2 internuclear axis onto the benzene plane makes an angle of 0° with respect to a C–C–C bond-angle bisector.

A rough picture of the intermolecular level structure of benzene–N_2 corresponding to the fitted IPS can be obtained by computing diagonal force constants for expected intermolecular modes and then using those force constants to estimate harmonic vibrational frequencies. One expects three intermolecular modes to be roughly harmonic: (a) a doubly-degenerate bend (ν_β), corresponding to relative translation of the N_2 and benzene moieties parallel to the benzene plane, (b) a singly degenerate stretch (ν_σ), corresponding to relative translation along the benzene C_6 axis, and (c) an N_2 libration (ν_θ), corresponding to hindered rotation of the N_2 moiety about an axis perpendicular to both its internuclear axis and to the benzene C_6 axis. For these modes one calculates harmonic frequencies of 44, 60, and 72 cm^{-1}, respectively. To obtain these values we took the relevant inertial factors to be $\sqrt{1/\mu+R^2/I_\perp}$ for the bend,[15] $\sqrt{1/\mu}$ for the stretch, and $\sqrt{1/I}$ for the libration, where μ is the reduced mass of the complex, $I_\perp$ is the moment of inertia of benzene perpendicular to its C_6 axis, and I is the moment of inertia of the N_2 moiety.

TABLE III. Inertial parameters for benzene–N_2 calculations.

Isotopomer	$I_\perp=\frac{I_\parallel}{2}$ [a]	I [b]	μ [c]
h_6-benzene–$^{14}N_2$	88.8773	8.473 385 5	20.604
h_6-benzene–$^{15}N_2$	88.8773	9.078 627	21.669 906
d_6-benzene–$^{14}N_2$	107.398	8.473 385 5	21.008 6

[a]The in-plane moment of inertia of benzene in amu Å^2.
[b]The moment of inertia of nitrogen in amu Å^2.
[c]The reduced mass of the complex in amu.

In addition to the aforementioned intermolecular vibrations, one also expects an intermolecular degree of freedom corresponding primarily to internal rotation/torsion of the N_2 about an axis perpendicular to its internuclear axis and parallel to the C_6 axis. From the fitted IPS the barrier to this motion is only 0.05 cm^{-1}. As such, one expects essentially free internal rotation corresponding to this degree of freedom, with an internal rotation constant $b\equiv(1/I+1/I_\parallel)/2 \simeq 2.1$ cm^{-1}, where $I_\parallel$ is the moment of inertia of benzene along its C_6 axis.

IV. CALCULATION OF INTERMOLECULAR STATES

A. Hamiltonian, basis set, procedures

The calculation of benzene–N_2 intermolecular states for this work proceeded as described in detail in Ref. 19. Briefly, the intermolecular rotational/vibrational Hamiltonian (rigid monomers assumed) was expressed in terms of the five coordinates fixing the position of the N_2 moiety relative to the benzene and referred to the BF_1 body-fixed axis system (i.e., z, ρ, Φ, θ, and ϕ, see Sec. II) and (b) three Euler angles fixing the orientation of BF_1 with respect to a space-fixed axis system. This Hamiltonian is readily expressed [see Eqs. (3.1) and (3.2) of Ref. 19] as the sum of a vibrational ($J=0$) term, H_v, and a rovibrational term, H_{rv}, the latter corresponding to the overall rotational motion of the complex as well as substantial Coriolis coupling terms. The only substantive difference between the Hamiltonian of this work and that of Ref. 19 is the IPS function employed. Here, we use the function V detailed in Sec. III above.

Intermolecular vibrational states were computed variationally by using filter diagonalization methods[33–35] to diagonalize the $J=0$ Hamiltonian. The Hamiltonian was expressed in a basis set fully symmetry-adapted to the G_{24} molecular symmetry group[36] of the complex. The functional form of the basis set, the parameters delineating its size, and the parameters defining the size of the grid on which matrix elements of V were computed, were all identical to those of Ref. 19. Monomer geometries were taken to be identical to those used for the *ab initio* calculations (see Sec. II). The inertial factors employed for the three isotopomers considered are given in Table III. Convergence of zero-point levels and the reliability of the computer code was checked by comparing the variationally calculated zero-point energies for h_6-benzene–$^{14}N_2$ (-403.72 cm^{-1}), h_6-benzene–$^{15}N_2$ (-405.68 cm^{-1}), and d_6-benzene–$^{14}N_2$ (-406.97 cm^{-1}) to values computed by rigid-body diffusion Monte Carlo (RBDMC).[37] Agreement between variational and RBDMC

results was found to within the statistical error of the RB-DMC calculations (± 0.5 cm^{-1}) for all three isotopomers. Notably, the zero-point energy of h_6-benzene–$^{14}N_2$ compares reasonably well with the experimental value of -323 ± 24 cm^{-1} obtained from measurements of the adiabatic ionization potential of benzene and the appearance potential of benzene$^+$ from photoionization of benzene–N_2.[13]

B. $J=0$ level structure

Table IV summarizes the results of calculations relating to the intermolecular level structures of perprotonated and predeuterated benzene–$^{14}N_2$ for the fitted IPS of Sec. III. The table includes all states <90 cm^{-1} above the zero-point levels. Assignments of the states were made on the basis of (a) the expectation values of geometrical quantities, as given in the table for the perprotonated species, (b) the basis-set composition of the eigenstates, and (c) the energy-level pattern of the states. Relevant to (b), one basis-set quantum number (l) is directly associated with van der Waals bending states, and a second (m) is associated with internal rotation states (see Ref. 19). Specifically, l is the quantum number associated with the component of angular momentum along the benzene C_6 axis due to the orbital motion of the monomers' centers-of-mass in BF_1. Associated with states having n quanta in a ''pure'' van der Waals bending mode are values of $|l|$ equal to one of the following: $n, n-2, n-4, \ldots$. m is the quantum number associated with angular momentum along C_6 arising from the rotation of the monomers about their individual centers-of-mass. A pure internal rotation state is characterized by a single value of m and by an energy equal to bm^2, with b defined in Sec. III C.

As indicated in Table IV, the $J=0$ level structure can be readily assigned in terms of a 37.1 cm^{-1} (35.1 for d_6) bending mode (ν_β, E_1^+), a 48.6 cm^{-1} (48.4 cm^{-1}) stretching mode (ν_σ, A_1^+), a 66.5 cm^{-1} (65.8 cm^{-1}) N_2 librational mode (ν_θ, A_1^-), and internal rotation structure with $b = 2.155$ cm^{-1} (2.137 cm^{-1}) built on states corresponding to quanta in these three modes. The computed fundamental frequencies of the three vibrational modes are quite reasonable in the light of the corresponding harmonic frequencies found for the fitted IPS in Sec. III C. Similarly, the internal rotation constant found in the $J=0$ calculations is close to that expected for free internal rotation about the C_6 axis in a complex for which $\theta = 90°$ and $\rho = 0$. While almost all of the assigned states are $>90\%$ pure with respect to the aforementioned modes as judged by the basis-set composition, some involve significant contributions from other zeroth-order levels. Such states are indicated in Table IV by placing their nominal assignments in parentheses.

C. Rotational constants

Intermolecular rovibrational states and energies and rotational constants obtained therefrom, were computed from $J=0$ states by the Eckart-frame transformation method presented first in Ref. 38 and applied directly to benzene–N_2 in Ref. 19. As pointed out in these works this method produces rovibrational eigenstates to the extent that rotation-vibration coupling terms in the full Hamiltonian are eliminated when that Hamiltonian is transformed to the Eckart frame. An assessment of the accuracy of rovibrational energies obtained by the Eckart method for benzene–N_2 is given in Ref. 19 for an IPS different than that employed herein. One expects similar accuracy to apply to the results reported below.

TABLE IV. Calculated properties of $J=0$ intermolecular states for perprotonated and perdeuterated benzene–$^{14}N_2$ isotopomers.

Irrep	Energy[a]/cm^{-1}	$\langle z\rangle$[b]/Å	Δz[c]/Å	$\langle\rho\rangle$[d]/Å	$\Delta(\cos\theta)$[e]	Assignment[f]
A_1^+	0	3.520	0.122	0.358	0.176	Zero-point
	48.62 (48.37)	3.592	0.215	0.441	0.189	ν_σ
	74.85 (71.01)	3.557	0.145	0.626	0.188	$2\nu_\beta$
	77.49 (76.88)	3.518	0.122	0.357	0.170	6
	82.77 (78.66)	3.575	0.149	0.691	0.186	$2\nu_\beta+2$
	87.13 (86.02)	3.565	0.269	0.472	0.192	$2\nu_\sigma$
A_2^+	77.49 (76.87)	3.518	0.122	0.357	0.170	6
	81.37 (77.28)	3.565	0.128	0.708	0.184	$2\nu_\beta+2$
B_1^+	46.95 (44.60)	3.542	0.125	0.549	0.178	$\nu_\beta+2$
	70.42 (68.42)	3.541	0.126	0.524	0.192	$\nu_\beta+4$
	86.80 (85.27)	3.593	0.162	0.523	0.264	$(\nu_\theta+3)$
B_2^+	46.78 (44.44)	3.541	0.125	0.549	0.178	$\nu_\beta+2$
	70.42 (68.42)	3.541	0.126	0.524	0.192	$\nu_\beta+4$
	86.75 (85.20)	3.594	0.163	0.525	0.263	$(\nu_\theta+3)$
E_1^+	37.13 (35.09)	3.537	0.125	0.540	0.182	ν_β
	46.43 (44.18)	3.546	0.125	0.545	0.181	$\nu_\beta+2$
	68.94 (68.12)	3.583	0.136	0.424	0.304	$\nu_\theta+1$
	73.28 (70.62)	3.543	0.125	0.552	0.176	$\nu_\beta+4$
	81.85 (79.67)	3.618	0.198	0.647	0.205	$\nu_\sigma+\nu_\beta$
	89.91 (87.68)	3.623	0.200	0.665	0.196	$\nu_\sigma+\nu_\beta+2$
E_2^+	8.62 (8.55)	3.519	0.122	0.328	0.175	2
	34.46 (34.19)	3.519	0.122	0.357	0.173	4
	57.27 (56.95)	3.592	0.215	0.441	0.187	$\nu_\sigma+2$
	73.18 (69.05)	3.563	0.129	0.707	0.183	$2\nu_\beta$
	83.02 (78.60)	3.568	0.131	0.717	0.181	$2\nu_\beta+2$
	83.21 (82.68)	3.590	0.214	0.446	0.184	$\nu_\sigma+4$
	85.59 (81.40)	3.575	0.151	0.630	0.186	$2\nu_\beta+2$
A_1^-	37.09 (35.25)	3.532	0.124	0.531	0.185	$\nu_\beta+1$
	66.49 (65.83)	3.583	0.136	0.418	0.305	ν_θ
	82.56 (80.53)	3.609	0.200	0.629	0.207	$\nu_\sigma+\nu_\beta+1$
A_2^-	42.25 (39.79)	3.551	0.125	0.556	0.178	$\nu_\beta+1$
	84.86 (82.47)	3.633	0.197	0.688	0.192	$\nu_\sigma+\nu_\beta+1$
B_1^-	19.39 (19.24)	3.519	0.122	0.357	0.174	3
	68.08 (67.68)	3.591	0.215	0.441	0.186	$\nu_\sigma+3$
	76.26 (71.97)	3.566	0.129	0.715	0.182	$2\nu_\beta+1$
B_2^-	19.38 (19.22)	3.519	0.122	0.357	0.174	3
	68.06 (67.66)	3.591	0.215	0.441	0.186	$\nu_\sigma+3$
	75.81 (71.56)	3.565	0.129	0.717	0.182	$2\nu_\beta+1$
E_1^-	2.16 (2.14)	3.519	0.122	0.358	0.176	1
	50.79 (50.51)	3.592	0.215	0.441	0.188	$\nu_\sigma+1$
	53.82 (53.40)	3.518	0.122	0.357	0.171	5
	73.91 (69.99)	3.557	0.133	0.678	0.185	$2\nu_\beta+1$
	79.97 (75.70)	3.577	0.147	0.654	0.183	$2\nu_\beta+1$
	88.81 (87.08)	3.560	0.262	0.495	0.194	$2\nu_\sigma+1$
E_2^-	39.98 (37.77)	3.540	0.125	0.545	0.180	$\nu_\beta+1$
	56.24 (54.12)	3.543	0.125	0.535	0.186	$\nu_\beta+3$
	57.94 (55.45)	3.542	0.125	0.551	0.177	$\nu_\beta+3$
	75.75 (74.81)	3.585	0.142	0.446	0.294	$\nu_\theta+2$
	84.72 (82.53)	3.618	0.192	0.634	0.212	$\nu_\sigma+\nu_\beta+1$
	88.70 (86.82)	3.541	0.130	0.512	0.199	$\nu_\beta+5$

[a]Energy above the zero-point level for the relevant isotopomer. Figures in parentheses pertain to the perdeuterated complex. All other numbers in the table refer to properties of the perprotonated species.
[b]The expectation value of z.
[c]The root-mean-squared deviation in z.
[d]The expectation value of ρ.
[e]The root-mean-squared deviation in $\cos\theta$. In all cases the expectation value of $\cos\theta$ equals zero.
[f]Bare integers in this column refer to the number of internal rotation quanta characterizing the state.

TABLE V. Calculated rotational constants (in cm^{-1}) of selected intermolecular vibrational states in benzene–N_2.

Isotopomer	Irrep	Energy[a]	B	A	$2A\lvert\zeta\rvert$
^{15}N	A_1^+	0	0.046 93 (0.047 019 2)[b]	0.095 43	0
^{14}N	A_1^+	0	0.048 72 (0.048 732)[c]	0.095 44	0
	E_1^-	2.16	0.048 70	0.095 43	0.1903
	E_1^+	37.13	0.047 95	0.096 06	0.0829
	E_1^+	46.43	0.047 76	0.096 08	0.2883
	A_1^+	48.62	0.047 25	0.095 73	0

[a]In cm^{-1} relative to the zero-point energy of the relevant complex.
[b]Value in parentheses is the experimentally derived quantity from Ref. 12.
[c]Value in parentheses is the experimentally derived quantity from Ref. 11.

Rotational constants from FT-microwave spectroscopy are available for the zero-point level of the perprotonated benzene–$^{15}N_2$ isotopomer in its ground state.[12] Vibronic spectroscopic results have provided analogous information for the ^{14}N isotopomer.[11] A comparison between these experimental values and rotational constants computed for the lowest-energy A_1^+ $J=0$ eigenstates of these two species is relevant to any assessment of the accuracy of our fitted IPS. Such a comparison is given in Table V. There is clearly good agreement between the experimental and computational results. Such agreement is consistent with the fact that the values of $\langle z\rangle = 3.502$ Å extracted from experiment are close to the 3.517 and 3.520 Å values computed for the ^{15}N and ^{14}N isotopomers, respectively.

Precise experimental values of benzene–N_2 ground-state rotational constants have not yet been measured for intermolecular levels other than zero-point levels. However, band contours observed in Raman spectroscopic experiments that we report on below do reflect the values of rotational constants for several higher-lying intermolecular states. Computed constants for these states are given also in Table V. We make use of some of these values below in band contour simulations designed to help justify assignments of observed Raman bands.

D. Calculated Raman intensities

Raman-scattering intensities for intermolecular bands were computed as described in Ref. 15. That is, intensities of intermolecular bands were quantified by the computation of scattering coefficients for parallel-polarized Raman fields. For the vibrational transition $v' \leftarrow v$ such a coefficient is given by

$$S_{v'v} \equiv 15|\langle v|\alpha_0^{(0)}|v'\rangle|^2 + 6\sum_{m=-2}^{2}|\langle v\,\alpha_m^{(2)}|v'\rangle|^2, \qquad (4.1)$$

where the $\alpha_m^{(j)}$ are spherical-tensor elements of the polarizability tensor operator measured with respect to the Eckart frame of the complex. The matrix elements appearing in Eq. (4.1) were calculated by using Eq. (5.2) of Ref. 38 under the assumption that the polarizability tensor of the benzene–N_2 equals the tensor sum of the permanent polarizability components of benzene and N_2 (taken from Refs. 30 and 39, respectively). The latter approximation, the validity of which is borne out by experimental results on numerous weakly bound complexes, takes the Raman scattering strength of an intermolecular band to arise entirely from the libration-induced modulation of the projection of the monomer-localized tensor components along Eckart axes embedded in the complex. One expects a reasonably good qualitative picture of the scattering spectrum of the complex to be obtained by this approach.

TABLE VI. Calculated scattering coefficients[a] for selected transitions between intermolecular levels in benzene–N_2.

Initial state	Final state	Transition frequency/cm^{-1}	$S_{v'v}$/Å^6
$0[A_1^+]$, 0 cm^{-1}	$2[E_2^+]$	8.62	0.269
	$\nu_\beta[E_1^+]$	37.13	0.596
	$\nu_\beta+2[E_1^+]$	46.43	0.056
	$\nu_\sigma[A_1^+]$	48.62	0.001
	$\nu_\theta+1[E_1^+]$	68.94	0.040
	$2\nu_\beta[E_2^+]$	73.18	0.002
	$2\nu_\beta[A_1^+]$	74.85	0.001
	$\nu_\sigma+\nu_\beta[E_1^+]$	81.85	0.001
$1[E_1^-]$, 2.16 cm^{-1}	$3[B_2^-]$	17.22	0.134
	$3[B_1^-]$	17.23	0.134
	$\nu_\beta+1[A_1^-]$	34.93	0.630
	$\nu_\beta+1[E_2^-]$	37.82	0.646
	$\nu_\beta+1[A_2^-]$	40.09	0.325
	$\nu_\sigma+1[E_1^-]$	48.63	0.002
	$\nu_\beta+3[E_2^-]$	54.08	0.020
	$\nu_\theta[A_1^-]$	64.33	0.068
	$2\nu_\beta+1[E_1^-]$	71.75	0.002
	$\nu_\theta+2[E_2^-]$	73.59	0.030
	$\nu_\sigma+\nu_\beta+1$, $[E_2^-]$	82.56	0.018

[a]See Eq. (4.1).

$S_{v'v}$ values were computed for two different initial states: the A_1^+ zero-point level and the $m=1$, E_1^- internal rotation level at 2.16 cm^{-1} above the zero-point. One expects only these states to be appreciably populated at the 1–2 K temperatures that apply to the seeded supersonic expansions that constitute the samples in experiments on benzene–N_2. At the same time, one expects that transitions originating in the zero-point level will contribute more prominently to any observed spectrum than the ones originating in the $m=1$ level owing to the factor of roughly 2 larger nuclear-spin statistical weights that apply to rotational levels of the former relative to those of the latter (for the ^{14}N isotopomer).

Table VI presents computed scattering coefficients associated with transitions from the two aforementioned initial states to other $J=0$ levels enumerated in Table IV. All such transitions with $S_{v'v} > 0.02$ Å,^{6} as well as other selected transitions, are included. There are several points of note in these results. First, bands involving unit change in the number of ν_β quanta are the most intense Raman bands. This is completely consistent with experimental and computational results reported previously on aromatic-rare gas complexes.[15,40] The intensity of such bands arises from the librational motion of the benzene (with its pronounced polarizability anisotropy) during the course of the bending vibration. Second, overtones of ν_β (e.g., the $E_2^+ \leftarrow A_1^+$ band at 73.18 cm^{-1} and the $A_1^+ \leftarrow A_1^+$ band at 74.85 cm^{-1}), though weak compared to a ν_β fundamental, nevertheless have computed intensities that are significant. This finding, too, is con-

sistent with observations and calculations pertaining to benzene–rare gas species.[40] Third, some bands gain significant scattering strength due to the fact that they involve a state that has acquired some pure ν_β character by vibrational coupling. For example, the E_1^+ upper state involved in the $E_1^+ \leftarrow A_1^+$ band at 46.43 cm^{-1}, while predominantly $\nu_\beta+2$ (see Table VI), also has about 9% ν_β character. As a result, the 46.43 cm^{-1} band steals some of the scattering strength of the strongly Raman-active ν_β fundamental. Fourth, after the ν_β fundamentals, the second-most intense bands are those that involve transitions wherein $|\Delta m|=2$. These are essentially one-dimensional rotational Raman transitions (internal rotation transitions) involving the N_2 moiety. They owe their intensity primarily to the polarizability anisotropy of that species, the same molecular property that determines the rotational Raman scattering strength of the isolated N_2 molecule. Finally, it is important to note that within the libration-induced approximation, only the anisotropic parts of the cluster's polarizability tensor produce Raman scattering strength;[15] the matrix elements involving $\alpha_0^{(0)}$ in Eq. (4.1) are all zero. Hence, those bands that could have a significant isotropic contribution to their scattering intensity (e.g., the $\nu_\sigma \leftarrow 0$ fundamental) have computed scattering coefficients that might well be significantly less than those that actually characterize them.

V. EXPERIMENT

Experimental results pertaining to the intermolecular Raman spectrum of the perprotonated and perdeuterated benzene–$^{14}N_2$ isotopomers were obtained by mass-selective ionization-detected stimulated Raman spectroscopies[41] (IDSRS). In such experiments the ground-state population changes induced in supersonic molecular-beam cluster samples by stimulated Raman transitions are probed by resonantly-enhanced multiphoton ionization (REMPI) followed by mass analysis of the photo-ions. A Raman transition is registered as a gain [ionization-gain stimulated Raman spectroscopy (IGSRS)] or a loss [ionization-loss stimulated Raman spectroscopy (ILSRS)] in mass-selected photo-ion signal as a function of Raman frequency, depending on the vibronic transition probed by the REMPI process.

The apparatus and general procedures employed for intermolecular IDSRS experiments in this laboratory have been described in detail elsewhere.[40] Here, we make note only of those specific conditions relevant to benzene–N_2. First, the molecular beam was generated by using a pre-expansion gas mixture consisting of helium, N_2, and benzene in the ratio of 100:1:1 at a total pressure of 300 psig. Second, most spectra were obtained by ILSRS with the REMPI field tuned to the 6_0^1 benzene-localized vibronic band of the complex at 38 603 cm^{-1} (38 781 cm^{-1} for the d_6 species), as assigned by Bernstein *et al.*[10] Third, in measuring all spectra the parent ion of the benzene–N_2 complex was the one that was detected. Fourth, the resolution of the Raman spectra, as determined by the bandwidths of the two stimulated-Raman driving fields, was 0.03 cm^{-1}. The resolution pertaining to the REMPI probe process was 0.3 cm^{-1}. Finally, one of the linearly-polarized stimulated-Raman driving fields was of sufficient intensity to generate optical-field-induced pendular states of benzene–N_2 species in the sample. As such, the contours of Raman bands observed in the IDSRS experiments are not rotational band contours, but pendular band contours. Band contour information was used in the assignment of intermolecular bands by comparing observed contours with contours simulated numerically according to the procedures outlined in Ref. 42. For these simulations the following parameters were used: rotational temperature of 2 K, aligning electric-field amplitude of 4×10^{10} W/cm^2, and polarizability anisotropy of benzene–N_2 of $\alpha_\perp-\alpha_\parallel=7\times10^{-40}$ $C^2\,m^2\,J^{-1}$. The temperature and the field amplitude are reasonable estimates of the conditions characterizing our experiments. The polarizability anisotropy is basically that of the benzene molecule. The rotational constants used in the simulations were taken from Table V, except where noted otherwise.

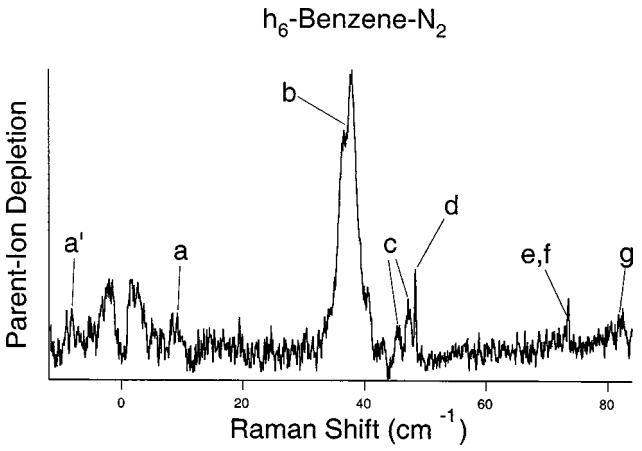

FIG. 1. Mass-selective ILSRS survey spectrum in the intermolecular region of the perprotonated benzene–N_2 complex. The spectrum was measured with parallel-polarized stimulated-Raman fields. Features discussed in the text are labeled. Features *a* and *a′* correspond to the same intermolecular band on opposite sides of the zero Raman shift.

VI. RAMAN SPECTROSCOPIC RESULTS

In a previous paper[15] intermolecular Raman spectra of benzene–N_2 isotopomers as measured by mass-selective ILSRS at 0.3 cm^{-1} resolution were reported. The principal result from that work was the observation of prominent, broad structure peaked near 37 cm^{-1} for the perprotonated ^{14}N isotopomer and corresponding structure peaked near 35 cm^{-1} for the perdeuterated ^{14}N isotopomer. These bands were assigned as the ν_β fundamental in the two species. The experiments reported here, corresponding to 0.03 cm^{-1} Raman resolution, reveal the presence of several weaker intermolecular Raman features for the these two isotopomers. Figure 1 shows a survey spectrum for the perprotonated species with features labeled for further reference. Figures 2–8 show expanded views of observed bands. Table VII summarizes all of the observed features for the two isotopomers. Also given in Table VII are assignments for the bands. Justification for these assignments is given in the following.

Consider first band *a* in the 8–9 cm^{-1} region (see Fig. 2), assigned as the $2\leftarrow0$ internal-rotation transition. This

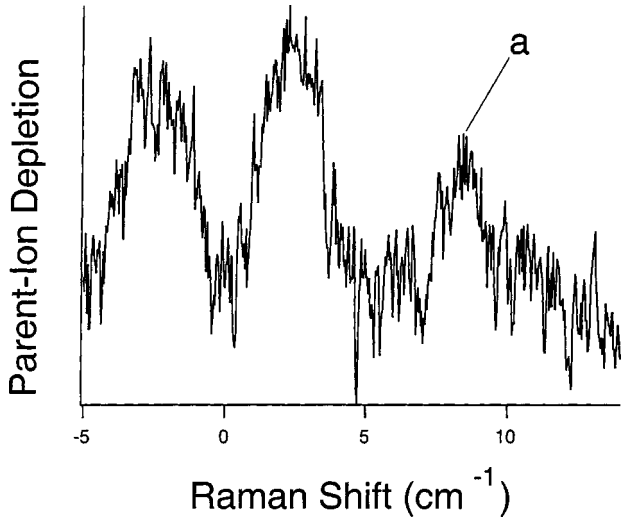

FIG. 2. Mass-selective ILSRS spectrum of perprotonated benzene–N_2 showing "rotational" Raman structure and the lowest frequency intermolecular band (*a*) observed near 8.6 cm^{-1}. The spectrum was measured with parallel-polarized stimulated-Raman fields.

band appears weakly, yet reproducibly above the noise, in the spectra of both isotopomers. Its assignment is straightforward based on several considerations. First, there is no reasonable basis on which to assign the band as anything other than an internal-rotation band. Its frequency is too low for it to be a transition in which the ν_σ, ν_β or ν_θ quantum number changes. Second, symmetry considerations preclude internal-rotation Raman transitions for which Δm is not even. Third,

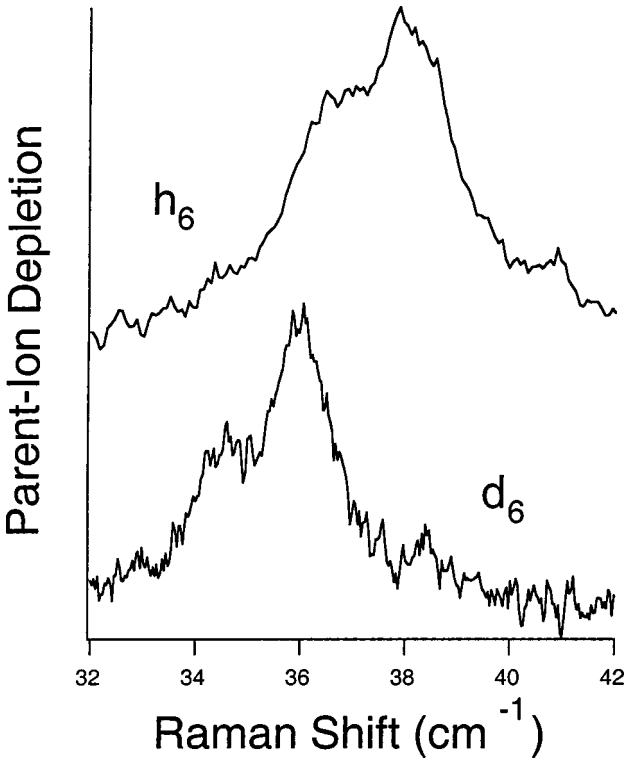

FIG. 3. Mass-selective ILSRS spectra of perprotonated and perdeuterated benzene–N_2 isotopomers showing expanded views of "band *b*" for the two species. Both spectra were measured with parallel-polarized stimulated-Raman fields.

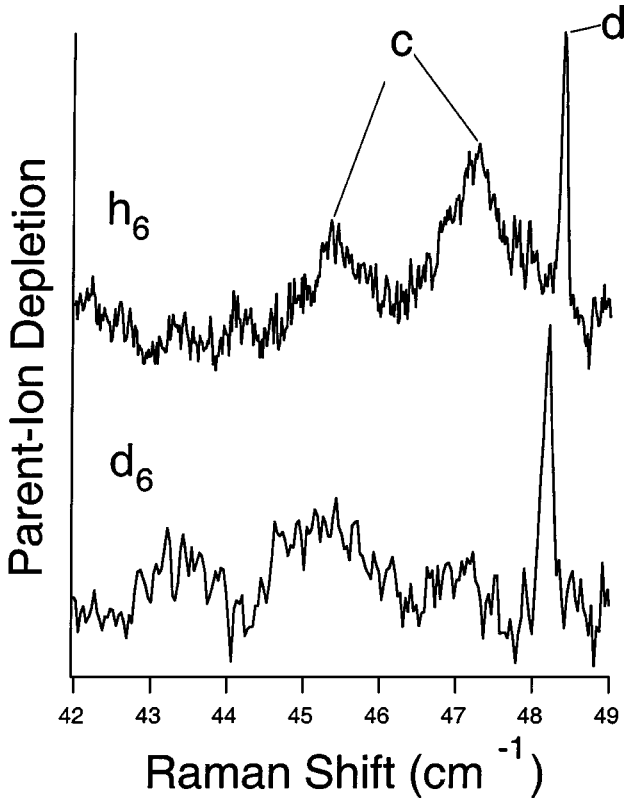

FIG. 4. Mass-selective ILSRS spectra of perprotonated and perdeuterated benzene–N_2 isotopomers measured with parallel-polarized stimulated-Raman fields in the region of bands *c* and *d*. The bands are labeled for the perprotonated species.

the results from high-resolution rotational spectroscopy,[11,12] clearly lead to the expectation of free, or nearly free, internal rotation characterized by an internal rotation constant $b \simeq 2.1\ cm^{-1}$ for both h_6 and d_6 isotopomers. This puts the $2 \leftarrow 0$ transition in the 8–9 cm^{-1} region for these species. Fourth, the observed band contours are consistent with a nontotally symmetric transition like $2[E_2^+] \leftarrow 0[A_1^+]$. Finally, the calculations of Sec. IV (see Table VI) predict a significantly intense $2 \leftarrow 0$ Raman band at 8.62 cm^{-1} (8.55 cm^{-1} for d_6), the only band calculated to be anywhere near the observed one. Though the observed band is weaker than might be expected (relative to band *b*, for example) based on the relative values of computed scattering coefficients, there are at least two plausible reasons why this might be so. These include the possibility of significant thermal population in the $m=2$ final level (not unreasonable given its small energy above the $m=0$ level) and the possible lack of complete vibrational-state selectivity in the REMPI probe step (due to spectral overlap of the $S_1 \leftarrow S_0$ vibronic bands originating in the $m=0$ and $m=2$ levels). Either possibility would serve to reduce the observed ILSRS intensity of the band.

Second, consider the intense structure corresponding to feature *b* in Fig. 1 (see Figs. 3 and 7 for expanded views) and assigned to bending fundamentals. There is little doubt that this assignment is substantially correct. First, the intermolecular Raman spectra of similar species—aromatic-rare gas complexes—are dominated by bending fundamentals as the strongest bands.[15,40] The strength of such bands arises from

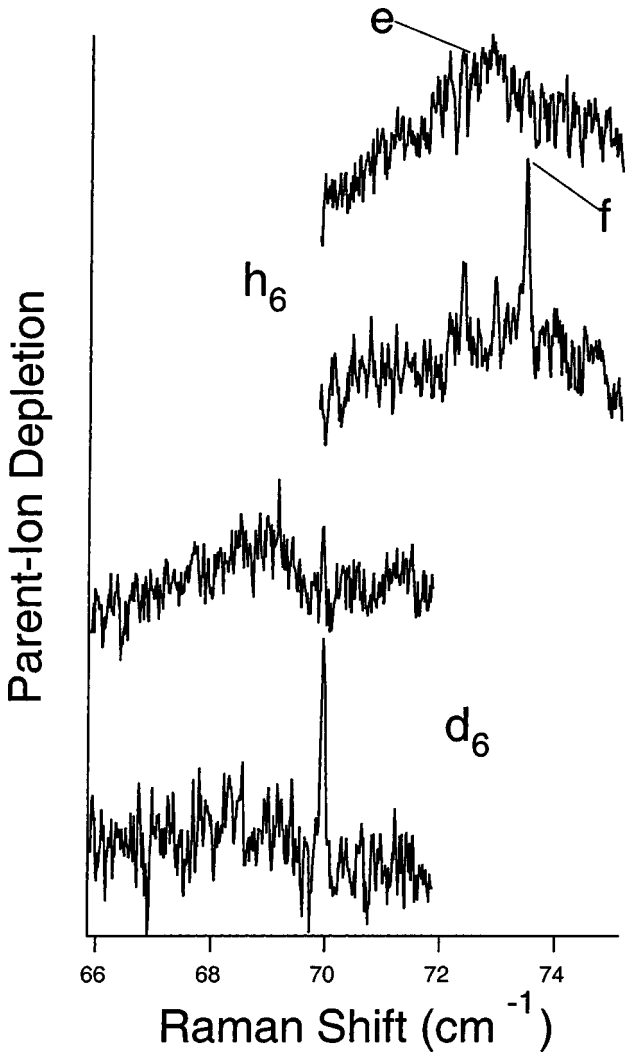

FIG. 5. Mass-selective ILSRS spectra of perprotonated and perdeuterated benzene–N_2 isotopomers in the region of bands *e* and *f*. For each isotopomer the top spectrum corresponds to perpendicularly-polarized stimulated Raman fields and the bottom spectrum to parallel-polarized fields. Bands *e* and *f* are labeled for the perprotonated species.

the libration-induced mechanism by virtue of the significant in-plane versus out-of-plane permanent polarizability anisotropy of the aromatic and the large librational amplitude of the aromatic during the course of the bending vibration. Second, the h_6-to-d_6 isotope shift of the structure is consistent with what one would expect for the bending mode. Approximating[15] the inertial factor associated with the bend as $\sqrt{1/\mu+R^2/I_\perp}$ and assuming harmonicity, one calculates a 7% shift to the red of the bending frequency upon perdeuteration, in line with the observations. Third, comparison of measured band contours with pendular contours simulated by using those rotational constants in Table V pertinent to the $\nu_\beta \leftarrow 0$ band reveals qualitative agreement (see Fig. 7). The extra, weaker structure in the experimental data that does not appear in the simulated contours (e.g., that marked by arrows in Fig. 7) is likely due to contributions to the experimental data from the three ν_β fundamentals originating out of the $m=1$ state, i.e., $(\nu_\beta+1)[A_1^-, A_2^-, E_2^-] \leftarrow 1[E_1^-]$. These bands should have Raman activities and frequencies similar to the $\nu_\beta \leftarrow 0$ band, though their contribution to any observed

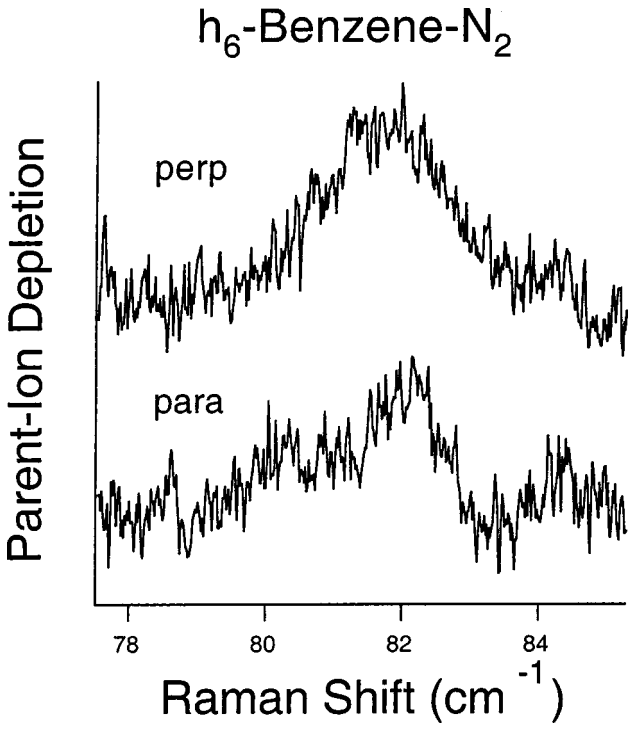

FIG. 6. Mass-selective ILSRS spectra of perprotonated benzene–N_2 in the region of band *g* as measured with perpendicular and parallel-polarized stimulated-Raman fields.

ILSRS spectrum might be expected to be considerably less than that of the latter band owing to (a) the factor-of-2 smaller statistical weights of the $m=1$ states relative to the $m=0$ ones and (b) a potential spectral bias in the probing of

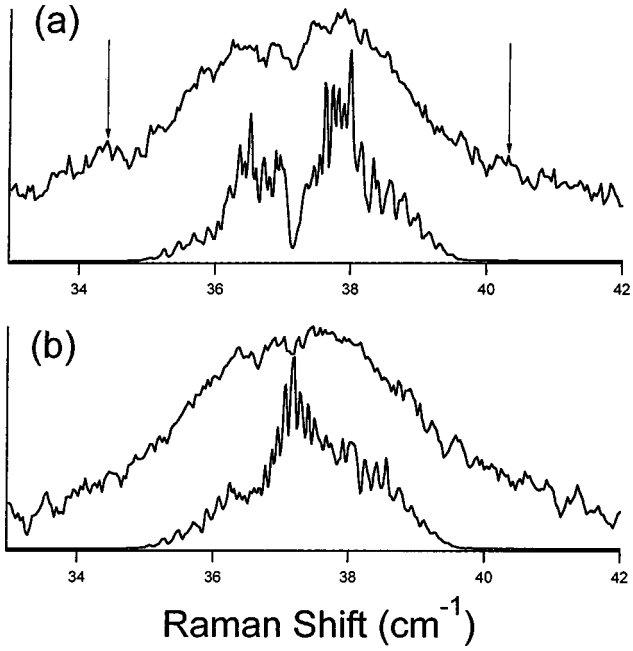

FIG. 7. Comparison of measured (top) and simulated (bottom) pendular contours associated with band *b* of perprotonated benzene–N_2 using (a) parallel- and (b) perpendicularly-polarized stimulated Raman fields. The parameters used to compute the simulated contours are given in the text and Table V and correspond to the $\nu_\beta \leftarrow 0$ band. The arrows in (a) are meant to highlight weak features in the measured spectra that are absent in the simulated contours.

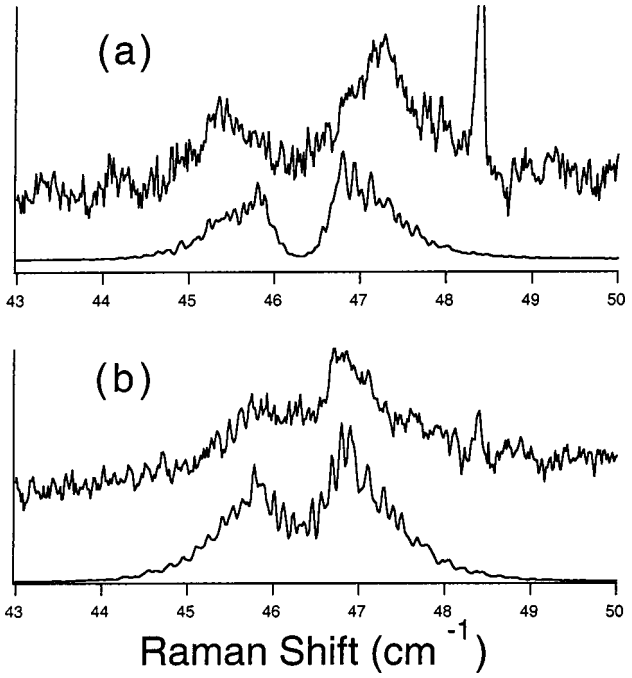

FIG. 8. Comparison of measured (top) and simulated (bottom) pendular contours associated with band *c* of perprotonated benzene–N_2 using (a) parallel- and (b) perpendicularly-polarized stimulated Raman fields. The parameters used to compute the simulated contours are given in the text and Table V and correspond to the $(\nu_\beta+2)[E_1^+]\leftarrow 0$ band.

$m=0$ species in the REMPI probe step of the IDSRS scheme. (The $m=0$ and $m=1$ 6_0^1 vibronic bands could be shifted from one another.) Finally, the excellent match between observed frequencies and Raman relative intensities in this region and those calculated for ν_β fundamentals in Sec. IV (see Table VI) is strong evidence for the correctness of the assignment.

We move next to bands *c* and *d* (see Figs. 4 and 8). That the observed structure does indeed correspond to two intermolecular bands rather than a single band contour is clear from the significantly larger h_6-to-d_6 isotope shift of the broad structure (*c*) at lower frequency relative to the sharp feature (*d*) at higher frequency. The assignment of band *d* as the ν_σ fundamental is quite firm. First, the dominant, sharp single peak and the marked drop in the intensity of that peak in going from parallel to perpendicular polarization [compare Fig. 8(a) top with 8(b) top], is just what one expects for the pendular band contour corresponding to a transition involving no change in vibrational symmetry, like the $A_1^+\leftarrow A_1^+$ ν_σ fundamental.[42] Second, the small h_6-to-d_6 shift of the band (0.5%) is consistent with the small isotope effect on the inertial factor, $\sqrt{1/\mu}$, associated with ν_σ. Finally, there is excellent agreement between the position of *d* and the h_6 and d_6 frequencies for ν_σ, as computed in Sec. IV. In regard to the assignment of band *c* as $(\nu_\beta+2)[E_1^+]\leftarrow 0$, several points are relevant. First, the 4% h_6-to-d_6 shift of the band clearly indicates the involvement of ν_β. Second, the band position for both isotopomers is where one would expect it to be given the observed frequencies for the ν_β fundamentals and the $(m=2)/(m=0)$ energy gap. Third, pendular band-contour simulations performed by using the calculated rotational constants for $(\nu_\beta+2)$ $[E_1^+]$ as upper and 0 $[A_1^+]$ as lower level (see Table V) yield a good match with the observed contours. Even better agreement is obtained by employing a Coriolis constant for $(\nu_\beta+2)$ $[E_1^+]$ slightly larger than the calculated value (i.e., $2A\zeta=0.32$ cm^{-1} rather than 0.2883 cm^{-1}). Such a comparison between calculated and observed contours is shown in Fig. 8. Finally, the calculations of Sec. IV predict the $(\nu_\beta+2)$ $[E_1^+]\leftarrow 0$ Raman band to be appreciably intense and to be very close to the observed frequency for both the h_6 and d_6 isotopomers.

TABLE VII. Observed intermolecular Raman bands in benzene–$^{14}N_2$.

Band frequency/cm^{-1}	Assignment
8.6(8.4)[a]	$2\leftarrow 0$
37.2(35.2)	$\nu_\beta\leftarrow 0$; $(\nu_\beta+1)\leftarrow 1$
46.5(44.6)	$(\nu_\beta+2)[E_1^+]\leftarrow 0$
48.4(48.1)	$\nu_\sigma\leftarrow 0$
72.8(68.7)	$2\nu_\beta[E_2^+]\leftarrow 0$
73.5(70.0)	$2\nu_\beta[A_1^+]\leftarrow 0$
81.7 (—)	$\nu_\beta+\nu_\sigma\leftarrow 0$

[a]Frequencies in parentheses correspond to bands of the perdeuterated complex.

Finally, consider the three weak bands *e*, *f*, and *g* observed in the frequency region beyond ~70 cm^{-1} (Figs. 5 and 6). It is clear from the observed broad band contours that *e* and *g* arise from nontotally symmetric vibrational transitions, whereas the sharp, strongly polarized contour observed for band *f* arises from a totally symmetric vibrational transition. Our assignment of these bands as *e*: $2\nu_\beta[E_2^+]\leftarrow 0$, *f*: $2\nu_\beta[A_1^+]\leftarrow 0$, and *g*: $(\nu_\beta+\nu_\sigma)\leftarrow 0$ is based on this band contour information as well as on the following. First, the analogous bands for the benzene–Ar complex have been observed in that species' intermolecular Raman spectrum. The expected similarity of the benzene–Ar and benzene–N_2 complexes with regard to their ν_β and ν_σ modes suggests that the three transitions should be observable in the latter complex's Raman spectrum, as well. Second, given the benzene–N_2 ν_β fundamental at 37.2 cm^{-1} and the ν_σ fundamental at 48.4 cm^{-1}, the observed positions of the three bands are close to where they would be expected for the $2\nu_\beta$ and $\nu_\beta+\nu_\sigma$ transitions in the harmonic approximation. Third, the h_6-to-d_6 isotope shifts of the bands *e* and *f* are consistent with them being bending overtones. (Band *g* for the d_6 isotopomer was observed only very weakly, and an accurate frequency for it, i.e., to within ± 1 cm^{-1}, was not obtained.) Finally, the calculations of Sec. IV predict the two $2\nu_\beta$ bands and the $\nu_\beta+\nu_\sigma$ band to be very close to the observed frequencies and to have observable Raman intensities.

In summary, the results of this section go a considerable way toward characterizing the intermolecular level structure of benzene–N_2 in the region near the IPS minimum. That level structure is built upon a bending mode of 37.2 cm^{-1} (for the perprotonated fundamental), a stretching mode of frequency 48.4 cm^{-1}, and free (or nearly so) internal rotation about the C_6 axis with internal-rotation constant $B=2.15$ cm^{-1}. The one intermolecular mode that the experimental results do not reveal is the N_2 libration. Nevertheless, the excellent agreement between the computational results of

Sec. IV and the whole body of experimental data pertaining to the benzene–N_2 interaction suggests that the computed fundamental frequency of 66.5 cm^{-1} for the libration is likely close to the actual value.

The present results should be considered in the light of other experimental studies of intermolecular vibrations in benzene–N_2. They are clearly consistent with the rotational results of Weber *et al.*[11] which point to the presence of free, or nearly free, internal rotation about the C_6 axis in the ground-state manifold of the complex. In regard to the other intermolecular modes, other data are limited. Oshima *et al.*[12] quote 26.5 cm^{-1} for ν_β and 45.6 cm^{-1} for ν_σ from centrifugal-distortion constants measured for benzene–$^{15}N_2$. The latter value is in rather good agreement with our benzene–$^{14}N_2$ ν_σ after accounting for the isotope shift. However, the ν_β value deviates significantly from ours. Given the indirect, model-dependent way in which vibrational frequencies are derived from distortion constants, such disagreement is not too surprising. Notably, the intermolecular frequencies of benzene–Ar obtained from microwave-measured centrifugal distortion constants (see Ref. 12) are in error in much the same way as their benzene–N_2 analogs, with ν_σ being close to the actual value[40] and ν_β being too low by about 40%. The only other experimentally measured intermolecular intervals reported for benzene–N_2 are from the vibronic spectra of Ref. 10 and pertain to the S_1 electronic-state manifold. Unfortunately, the assignment of these intervals is not clear. The R2PI spectra in which they occur likely have some contamination from resonances of benzene–$(N_2)_n$, $n>1$ clusters and/or from hot bands of the 1:1 species. Further, the possibility that internal rotation about C_6 might be significantly less free in the S_1 manifold than in S_0 complicates the assignment of the R2PI structure. Still, one band observed 37 cm^{-1} to the blue of the 6_0^1 origin is the most intense band in that spectrum, aside from the 6_0^1 band itself and associated sequence/hot bands. Given our ground-state results it is reasonable to suppose that this 37 cm^{-1} interval corresponds to ν_β in S_1.

VII. CONCLUSION

Comparison of all the available experimental data on the ground-state properties of benzene–N_2—intermolecular transition energies, rotational constants, binding energy—with the calculated results of Sec. IV reveals excellent agreement in almost all particulars (see Tables V, VI, and VII). Prior work on benzene–Ar clearly demonstrated the good performance of the CCSD(T) method in computing IPS points for that species with the aug-cc-pVDZ-33211 basis. The results of the present work provide additional compelling evidence that *ab initio* calculations at this level, even with a significantly limited set of IPS grid points, are accurate enough to facilitate assignment of experimental low-temperature spectra. In the case of benzene–N_2 this accuracy has been instrumental in the interpretation of experimental features whose assignments were otherwise in question and in confirming the assignment of more readily interpreted features. One concludes that with careful selection of grid points *ab initio* methodology of the type employed in this work, along with dynamically exact solution of the intermolecular Schrödinger equation, is likely to become an important tool in future investigations of large van der Waals complexes.

ACKNOWLEDGMENTS

The work at UCLA was supported by the U.S. Department of Energy and by the U.S. National Science Foundation. The work in Santiago was supported by the EU-TMR network ''Molecular Properties and Molecular Materials'' (Contract No. HPRN-CT-2000-00013) and by the Spanish Comisión Interministerial de Ciencia y Tecnología (PB98-0609-C04-01). H.K. acknowledges the Carlsberg Foundation.

[1] S. Leutwyler and J. Boesiger, Chem. Rev. **90**, 489 (1990).
[2] Th. Weber and H. J. Neusser, J. Chem. Phys. **94**, 7689 (1991).
[3] H. Koch, B. Fernández, and O. Christiansen, J. Chem. Phys. **108**, 2784 (1998).
[4] H. Koch, B. Fernández, and J. Makarewicz, J. Chem. Phys. **111**, 198 (1999).
[5] B. Fernández, H. Koch, and J. Makarewicz, J. Chem. Phys. **111**, 5922 (1999).
[6] B. Fernández, H. Koch, and J. Makarewicz, J. Chem. Phys. **110**, 8525 (1999).
[7] T. B. Pedersen, B. Fernández, H. Koch, and J. Makarewicz, J. Chem. Phys. **115**, 8431 (2001).
[8] C. Leforestier, L. B. Braly, K. Liu, M. J. Elrod, and R. J. Saykally, J. Chem. Phys. **106**, 8527 (1997).
[9] W. Kim, D. Neuhauser, M. R. Wall, and P. M. Felker, J. Chem. Phys. **110**, 8461 (1999).
[10] R. Nowak, J. A. Menapace, and E. R. Bernstein, J. Chem. Phys. **89**, 1309 (1988).
[11] Th. Weber, A. M. Smith, E. Riedle, H. J. Neusser, and E. W. Schlag, Chem. Phys. Lett. **175**, 79 (1990).
[12] Y. Ohshima, H. Kohguchi, and Y. Endo, Chem. Phys. Lett. **184**, 21 (1991).
[13] B. Ernstberger, H. Krause, and H. J. Neusser, Z. Phys. D: At., Mol. Clusters **20**, 189 (1991).
[14] V. A. Venturo, P. M. Maxton, and P. M. Felker, J. Phys. Chem. **96**, 5234 (1992).
[15] P. M. Maxton, M. W. Schaeffer, S. M. Ohline, W. Kim, V. A. Venturo, and P. M. Felker, J. Chem. Phys. **101**, 8391 (1994).
[16] P. Hobza, O. Bludský, H. L. Selzle, and E. W. Schlag, J. Chem. Phys. **98**, 6223 (1993).
[17] T. Wesolowski, O. Parisel, Y. Ellinger, and J. Weber, J. Phys. Chem. A **101**, 7818 (1997).
[18] T. Wesolowski, Y. Ellinger, and J. Weber, J. Chem. Phys. **108**, 6078 (1998).
[19] P. M. Felker, J. Chem. Phys. **114**, 7901 (2001).
[20] S. F. Boys and F. Bernardi, Mol. Phys. **19**, 553 (1970).
[21] Th. Weber, A. von Bargen, E. Riedle, and H. J. Neusser, J. Chem. Phys. **92**, 90 (1990).
[22] J. M. Hollas, *Modern Spectroscopy*, 3rd ed. (Wiley, New York, 1987).
[23] See EPAPS Document No. E-JCPSA6-118-009303 for the coordinates of the grid points and the values of the *ab initio* interaction energies. This document may be received via the EPAPS homepage (http://www.aip.org/pubservs/epaps.html) or from ftp.aip.org in the directory /epaps/. See the EPAPS homepage for more information.
[24] K. Raghavachari, G. W. Trucks, J. A. Pople, and M. Head-Gordon, Chem. Phys. Lett. **157**, 479 (1989).
[25] T. Helgaker, H. J. Aa. Jensen, P. Jørgensen *et al.*, DALTON, a molecular electronic structure program, Release 1.2, 2001. See http://www.kjemi.uio.no/software/dalton/dalton.html
[26] H. Koch, A. S. de Meras, T. Helgaker, and O. Christiansen, J. Chem. Phys. **104**, 4157 (1996).
[27] H. Koch, P. Jørgensen, and T. Helgaker, J. Chem. Phys. **104**, 9528 (1996).
[28] T. Brupbacher, J. Makarewicz, and A. Bauder, J. Chem. Phys. **101**, 9736 (1994).
[29] For example, B. N. Battacharya and N. Gordy, Phys. Rev. **119**, 144 (1960).
[30] M. R. Battaglia, A. D. Buckingham, and J. H. Williams, Chem. Phys. Lett. **78**, 421 (1981).

[31] P. R. Bevington, *Data Reduction and Error Analysis for the Physical Sciences* (McGraw–Hill, New York, 1969).
[32] For example, S. K. Kim, S. Li, and E. R. Bernstein, J. Chem. Phys. **95**, 3119 (1991).
[33] (a) D. Neuhauser, J. Chem. Phys. **93**, 2611 (1990); (b) **100**, 5076 (1994).
[34] M. R. Wall and D. Neuhauser, J. Chem. Phys. **102**, 8011 (1995).
[35] V. A. Mandelshtam and H. S. Taylor, J. Chem. Phys. **106**, 5085 (1997).
[36] A. J. Gotch and T. S. Zwier, J. Chem. Phys. **96**, 3388 (1992).
[37] V. Buch, J. Chem. Phys. **97**, 726 (1992).
[38] P. M. Felker, D. Neuhauser, and W. Kim, J. Chem. Phys. **114**, 1233 (2001).
[39] C. E. Dykstra, S.-Y. Liu, and D. J. Malik, Adv. Chem. Phys. **75**, 37 (1989).
[40] W. Kim and P. M. Felker, J. Chem. Phys. **107**, 2193 (1997).
[41] P. M. Felker, P. M. Maxton, and M. W. Schaeffer, Chem. Rev. **94**, 1787 (1994).
[42] W. Kim and P. M. Felker, J. Chem. Phys. **108**, 6763 (1998).